



Flow visualization of wave-type vortex generators having inline fin-tube arrangement

Chi-Chuan Wang^{a,*}, Jerry Lo^b, Yur-Tsai Lin^b, Min-Sheng Liu^a

^a Industrial Technology Res. Institute, D400 ERLITRI Bldg. 64, 195-6 Section 4, Chung Hsing Road, Chutung, Hsinchu 310, Taiwan

^b Department of Mechanical Engineering, Yuan-Ze University, Taoyuan, Taiwan

Received 16 May 2001

Abstract

This study presents visual observation of enlarged fin-and-tube heat exchangers with and without the presence of vortex generators. Three samples of fin-and-tube heat exchanger having inline arrangements are examined, including one plain fin and two wave-type vortex generators. For plain fin geometry at $Re = 500$, the horseshoe vortex generated by the tube row is not so pronounced, and a very large secondary flow circulation is seen between the first and second row. This flow re-circulation phenomenon is almost disappeared with the presence of proposed vortex generators. The presence of vortex generators significantly increase the vortical motions of the horseshoe vortices hitting on the tubes. A much better mixing characteristics is seen by introducing the vortex generators. The frictional penalty of the proposed vortex generators are about 25–55% higher than that of the plain fin geometry. The penalty of pressure drops of the proposed vortex generators relative to plain fin geometry is relatively insensitive to change of Reynolds number. © 2002 Elsevier Science Ltd. All rights reserved.

Keywords: Vortex generator; Fin-and-tube heat exchanger

1. Introduction

Vortex generators have generally been applied as a post-design method in aircraft applications to tackle a problem that was unexpected or not amenable to reliable operation. For aircraft applications, exploitation of vortex generators is mainly to prevent boundary layer separation and drag reductions (such as wedge, plough, ramp, scoop, dome, wheeler, wing, and wave type, [1]). The vortex generators often take the forms of small protrusions which may be incorporated into the main surface by embossing, stamping, punching, or attaching. Fig. 1 shows the commonly employed vortex generators. Swirl flow is generated as the mainstream flows across the small protrusions. Usually the vortical motions may be classified as

transverse and longitudinal vortices. The axis of a transverse vortex lies perpendicular to the flow direction while longitudinal vortices have their axes parallel to the main flow direction. The longitudinal vortex flow may swirl around the primary flow and exhibits three-dimensional characteristics. In general, longitudinal vortices are more effective than transverse vortices from the heat transfer perspective [2].

In recent years, the exploitation of vortex generators in compact heat exchangers application had received a lot of attentions. It is well known that enhanced surfaces are often employed in compact heat exchangers to effectively improve the overall heat transfer performance. Fiebig [3] points out that there are three major heat transfer enhancement mechanisms of enhanced surfaces, namely: (1) developing boundary layers, (2) swirl or vortices, and (3) flow destabilization or turbulence intensification. A recent technology review article in connection to patents by Wang [4] clearly shows that the most common enhanced surfaces are the interrupted surfaces in the form such as slit, offset strip, and louver.

*Corresponding author. Tel.: 886-35-916-294; fax: 886-35-820-250.

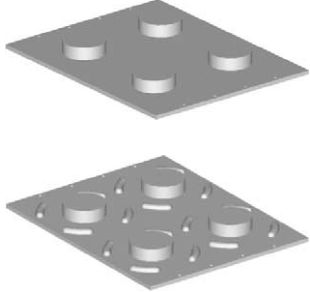
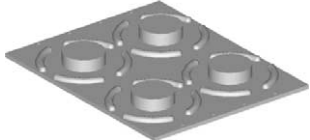
E-mail address: ccwang@itri.org.tw (C.-C. Wang).

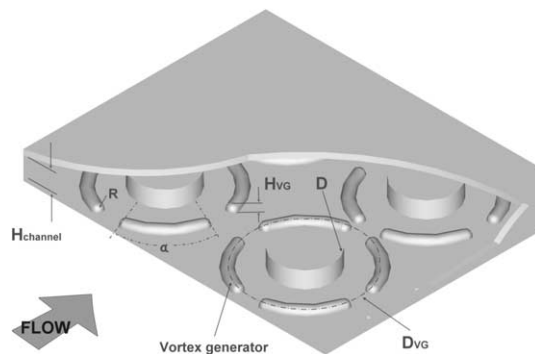
Nomenclature		R	radius of curvature of the vortex generator (m)
α	angular angle of the vortex generator (deg.)	Re	Reynolds number based on channel height, dimensionless
A_c	cross-section area (m ²)	ΔP_{int}	pressure drops for interrupted surface (Pa)
H_{OV}	height of vortex generator (m)	ΔP_{Plain}	pressure drops for plain fin geometry (Pa)
D	tube outer diameter (m)	ΔP_{VG}	pressure drops for vortex generator (Pa)
D_{VG}	outer diameter of vortex generator (m)	α	angular angle of the vortex generator degree
P	periphery of the cross-section area (m)		

Though interrupted surfaces can significantly improve the heat transfer performance, the associated penalty of pressure drop is also tremendous. In contrast to the common interrupted surfaces, the vortex generator not only improves the heat transfer performance via

all the three heat transfer mechanisms but also reveals comparatively small pressure drops. This is because wall friction is related to the derivative of streamwise velocity but spanwise and normal velocities. The vortex generators characterized the secondary flow pattern from the

Table 1
Configuration of the test sample and the definitions of geometrical parameters of vortex generators

	$H_{channel}$ (mm)	D (mm)	H_{VG} (mm)	α	R (mm)	D_{VG} (mm)	
Plain							Base
VG1	15	50.2	5	30°	5.0	100.2	
VG5				60°	5.0	100.2	



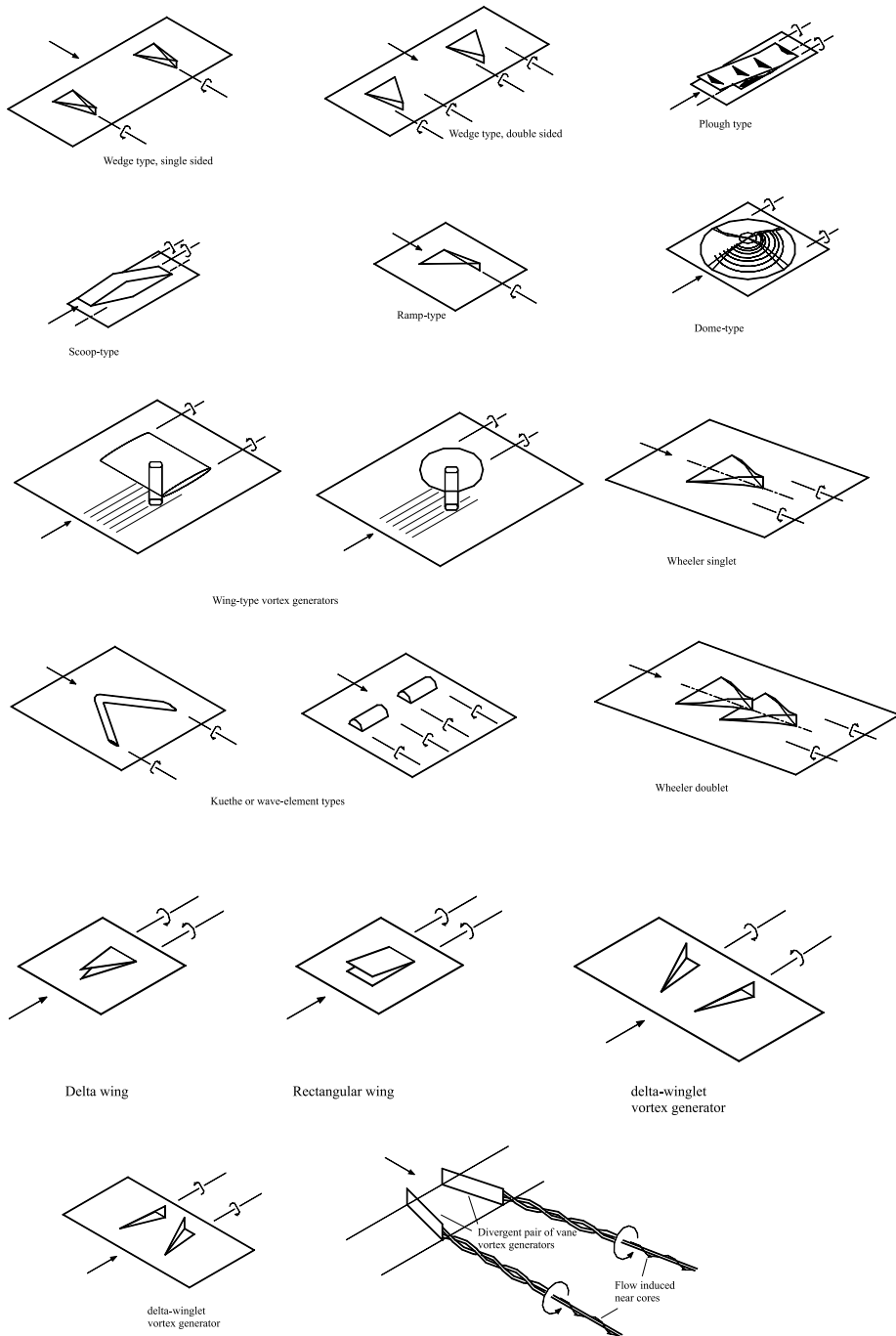


Fig. 1. Various types of vortex generators.

vortical motions that is caused by the spanwise and normal velocities. Heat transfer enhancement is associated with the secondary flow but with small penalty of wall friction [5]. Therefore, longitudinal vortices are recognized especially suitable for heat transfer applications. The first literature reporting the heat transfer

performance improvements is by Edwards and Alker [6]. They reported the local average heat transfer coefficient was about 40% higher than that of plain fin surface. For applications to the compact heat exchangers with vortex generators, Fiebig and his coworkers [7–10] had conducted very comprehensive studies in association with

the influence of wing type, delta-wing type vortex generators. Very detailed information was reported about these kind of vortex generators. In this study, focus is made on the feasibility of the new type vortex generator that is especially appropriate for the common fin-and-tube heat exchangers.

2. Experimental setup

Experiments are performed in a water tunnel as depicted in Fig. 2. As shown in Fig. 2(a), city water is supplied to the water tank, the water flows through in series to the contraction section, damping screen, the calming section, test section, exit contraction section, flow meter, water pump, and the connection pipe line to complete the cycle. The test section is made of transparent acrylic having a cross-section of $254 \text{ mm} \times$

15 mm. Flow visualization is performed via dye-injection technique. Two needles that are capable to inject color dye are placed at the entrance of the inlet section. For further investigating the flow phenomenon inside the heat exchanger, the injection port can be either located in the center or near the wall to keep track the trajectory behaviors (Fig. 2(b)). Additional dye injection port is placed at the rear of the acrylic tube to observe the flow motion of the inert region behind the tube. The color in front of the test section is red whereas the color behind the tube is blue. A total of three acrylic test sections were made and tested. Their detailed geometrical parameters and relevant definitions of the vortex generators are shown in Table 1. The test samples include a plain fin configuration and two wave-element vortex generators. Notice that the tube layouts for the test samples are all inline arrangement. The outer tube diameter is

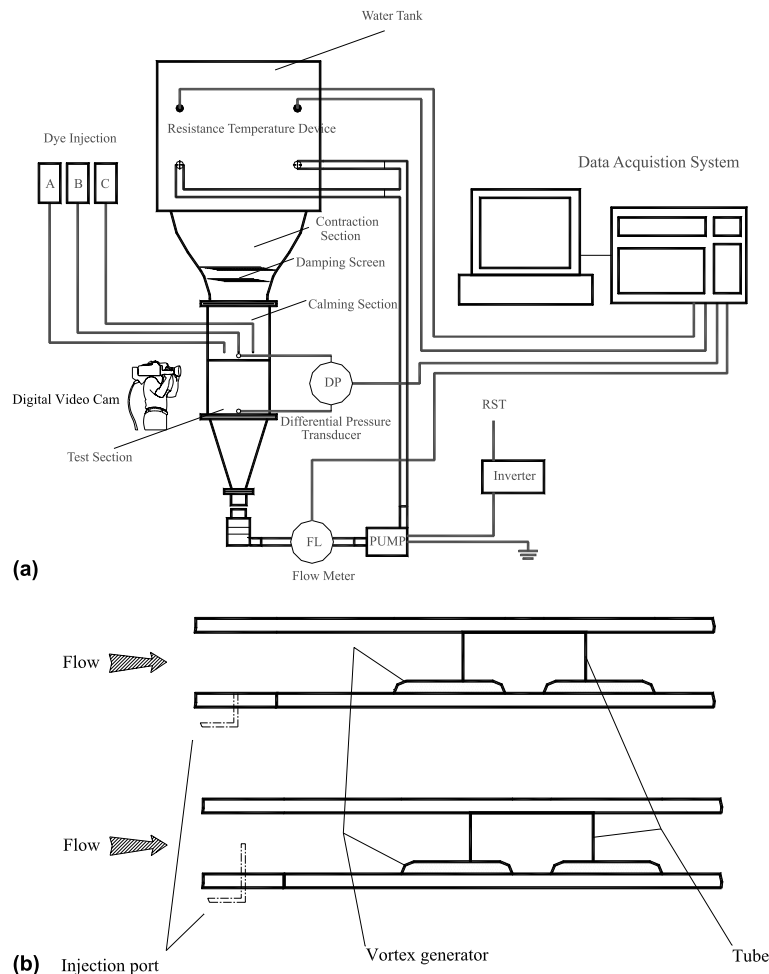


Fig. 2. Schematic of: (a) the test facility; (b) the arrangements of the injection port.

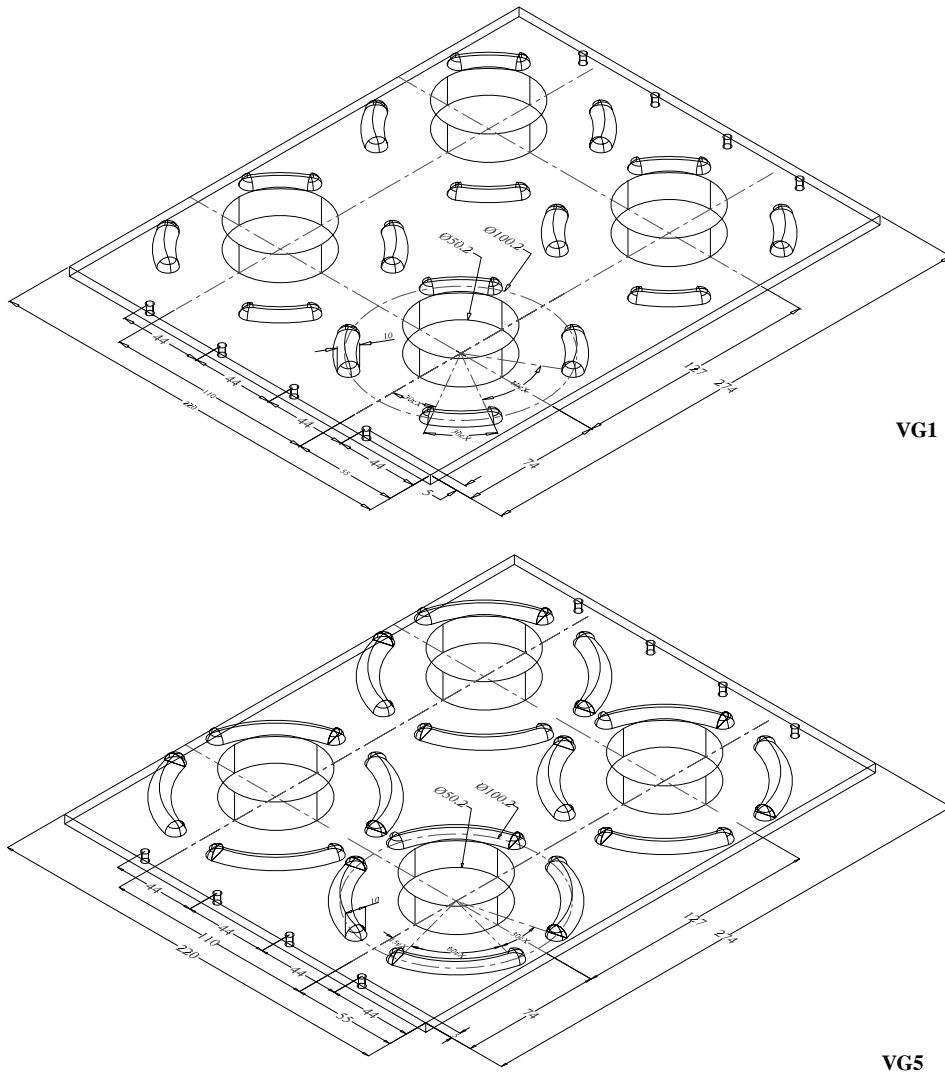


Fig. 3. Detailed geometric parameters of the vortex generator.

50.2 mm, and the channel height of the test section is 15 mm. The height of the vortex generator H_{VG} and its corresponding annular diameter D_{VG} are 5 and 100.2 mm, respectively. Detailed geometry of the vortex generators is seen from Fig. 3. Notice that the annular vortex angle for VG5 is 60° compared to 30° of VG1.

A digital video cam is placed outside the test section to record the trajectory of the injected dye. The water flow rate was measured by a very accurate magnetic flowmeter with a calibrated accuracy of 0.002 l/s. The pressure drops across the test section was measured by a precision pressure transducer (YOKOGOWA EJ110). Resolution of this pressure differential pressure transducer is 0.3%. The water temperature inside the tank

was measured by resistance temperature device (Pt100 Ω) having a calibrated accuracy of 0.1 $^\circ\text{C}$.

3. Results and discussion

Fig. 4 shows the flow visualization of plain fin geometry with Reynolds numbers of 500, 1500, and 3300. Notice that the Reynolds number is based on the hydraulic diameter of $4A_c/P$. As shown in Figs. 4(b) and (c) the injected dye in front of the tube hits the round tube and twisted back a little and then swirls surrounding the round tube to the next row (see Fig. 4(a)). The horseshoe vortex motion is not so oblivious at this low Reynolds number. The injected

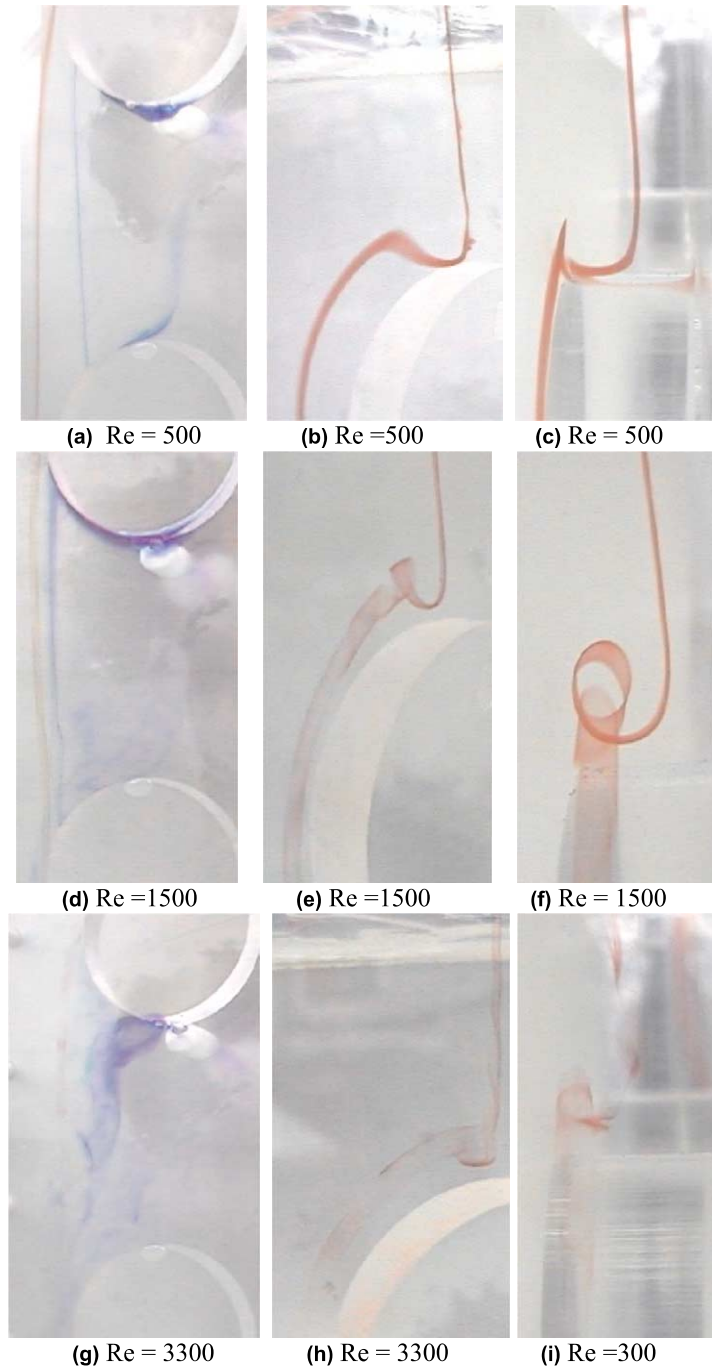


Fig. 4. Flow visualization of the plain fin geometry at $Re = 500, 1500,$ and 3300 .

dye (blue) right behind the first tube row climbs up the periphery of the tube, and then separated from the tube at an angle of approximate 110° (counting from the stagnation point of the first row). The trajectory of the blue dye then travels from the first row toward

the second row. It is interesting to note that the blue dye then turns around and goes back to the first row forming a huge circulation zone. This huge re-circulation zone implies a very poor heat transfer characteristics in this region. As the Reynolds number is

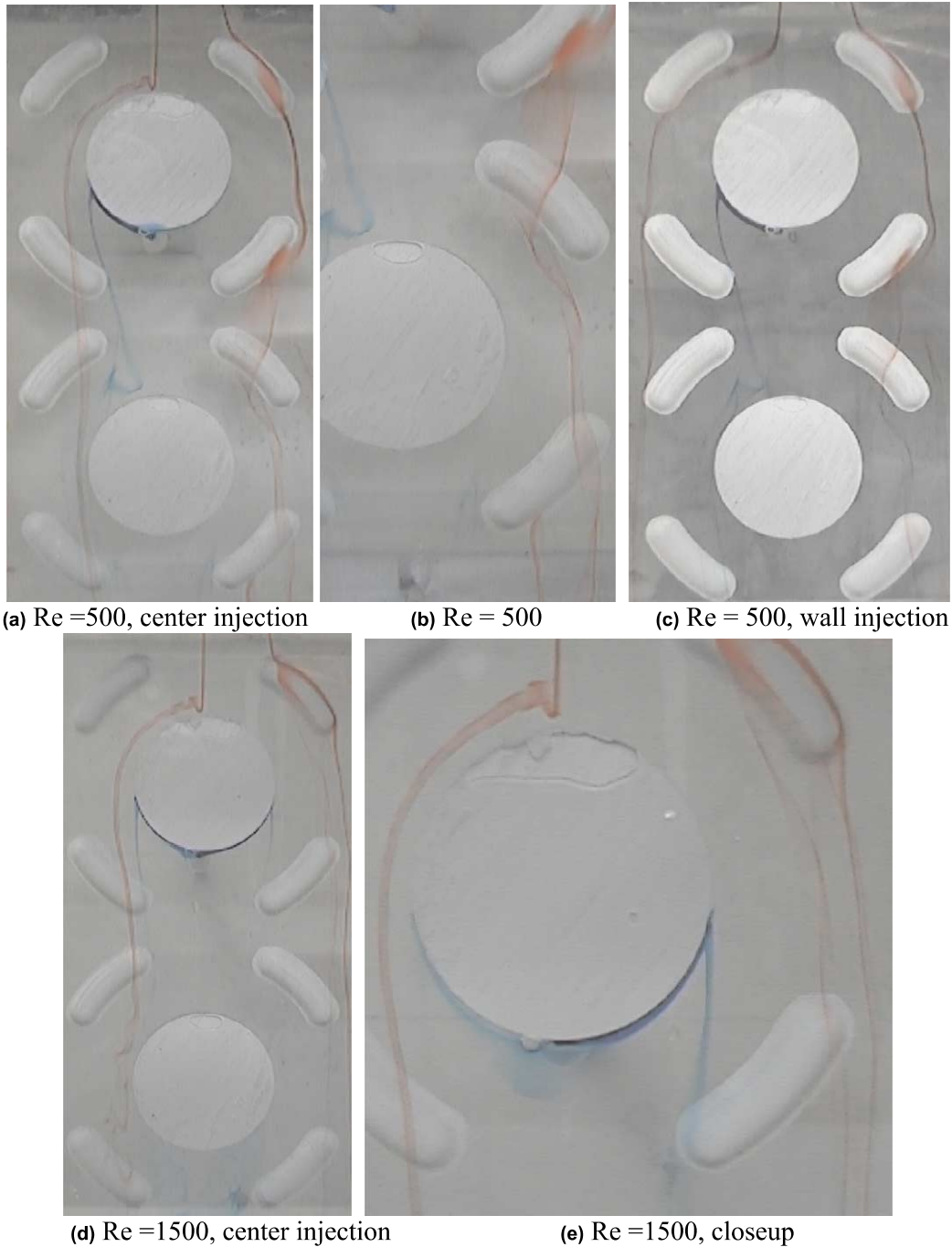


Fig. 5. Flow visualization of the VG1 vortex generator at $Re = 500$, 1500, and 3300.

further increased to 1500, one can clearly see in Figs. 4(e) and (f) that the horseshoe vortices is clearly formed and flows following a similar trajectory like $Re = 500$ to the second row. The injected blue dye still forms a re-circulation cycle that is even larger than

that of $Re = 500$. However, one can see the gap distance between the blue and the red dye is much closer than that of $Re = 500$. Apparently, this is due to the contribution of the horseshoe vortex that bring closer the blue dye. In addition, one can see a very small

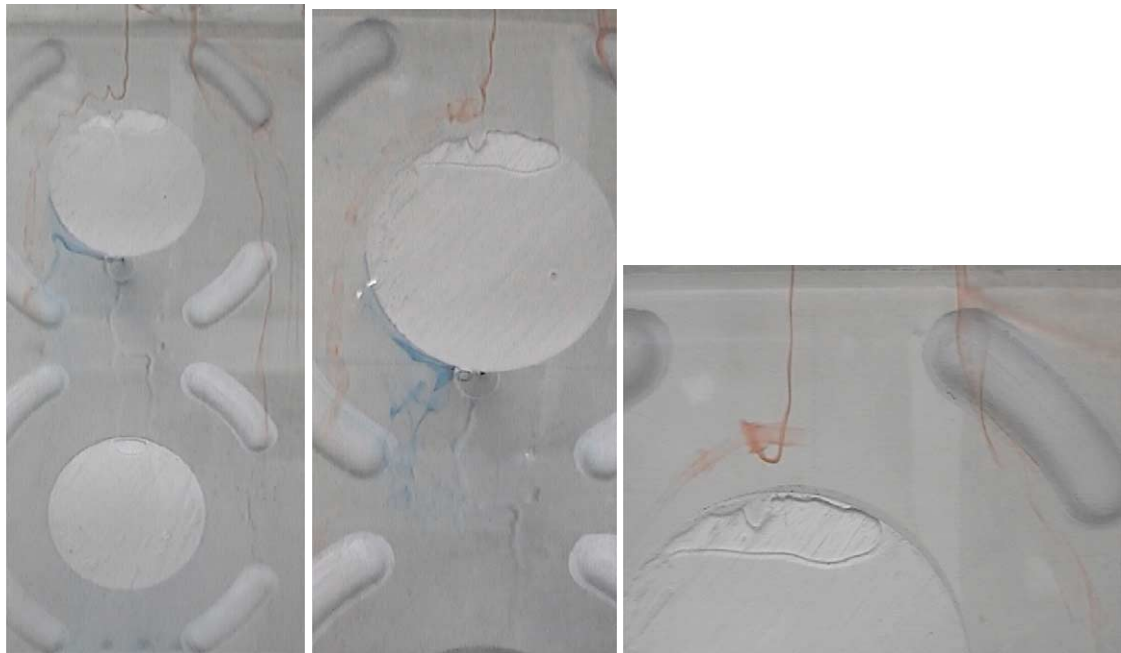
(f) $Re = 1500$, wall injection(g) $Re = 1500$, closeup(h) $Re = 3300$, center injection(i) $Re = 3300$ (j) $Re = 3300$

Fig. 5. (Continued)

amount of the blue dye was entrained to the vortex stream (red dye). A further increase of the Reynolds number to 3300, one can see the intensity of the horseshoe vortex is so strong that causes the shedding of the blue circulation zone (Figs. 4(g)–(i)).

With the presence of vortex generator VG1, it may be expected that the flow trajectory may be quite different. Fig. 5 shows the visual results of $Re = 500$, 1500, and 3300, respectively. For the injection located at the center position, one can see the horseshoe vortex in front of the

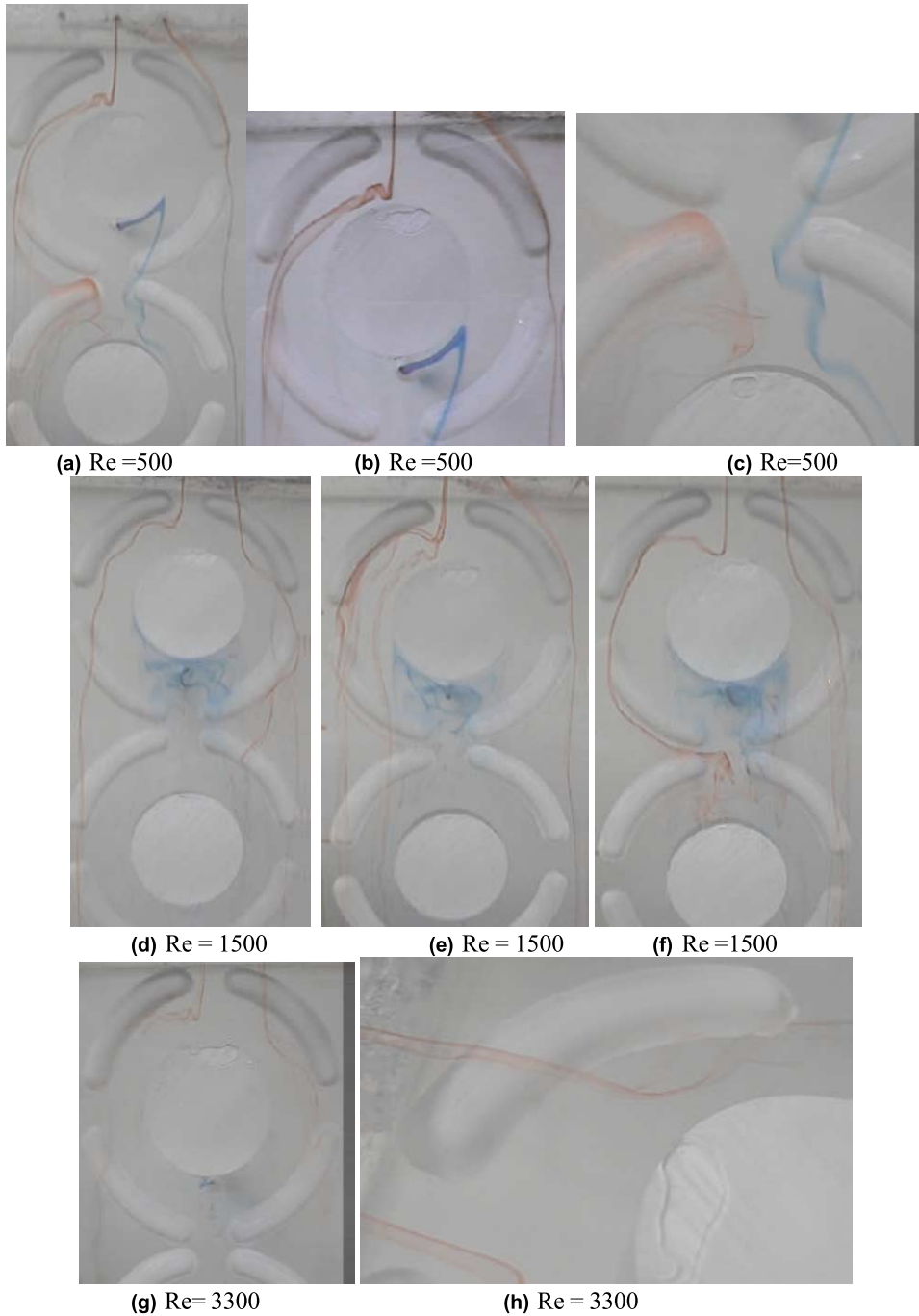


Fig. 6. Flow visualization of the VG5 vortex generator at $Re = 500, 1500,$ and 3300 .

first tube is intensified by the presence of vortex generator when compared to that in plain tube at $Re = 500$. Interestingly, the flow circulation behind the first row is interrupted. As seen in Fig. 5(a), the trajectory of the blue dye first climbs up the first row then departs at

approximate 100° and travels along the tangential direction of the trailing edge of the vortex generator to the second row. The blue dye then hits the second row and bounce back. However, unlike those shown in plain fin geometry, the bounced back blue dye was directed to the

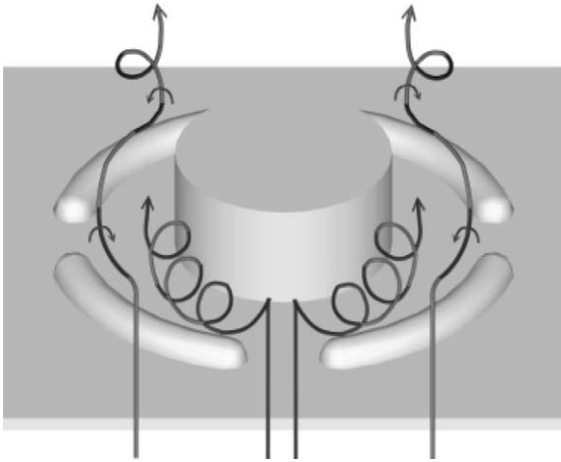


Fig. 7. Schematic of the flow motions across the vortex generators.

horseshoe vortex from the first row and does not circulate back to the first row. The results implies the inert heat transfer characteristics behind the tube is significantly improved at this low Reynolds number with the presence of vortex generators.

In the mean time, if the injection position is placed near the wall as shown in Fig. 5(c), after passing through the first generator, the trajectory of the red dye turns around instead of hitting the tube. The red dye then flows through the concave of the first vortex generator and flows surrounding the vortex generators towards downstream. The results may be related to the presence of vortex stream that flows across the vortex generator. As can be seen from the injected dye that is directly hitting the vortex generator, the flow

shows a complicated vortical motions. In this connection, the vortex is in fact a low pressure region, and this eventually will bring in the ambient fluid. Thus we can see that the circulation of the blue dye was interrupted by the vortex and was entrained into the vortex flow. This phenomenon can be further made clear in Figs. 5(d)–(g). With a higher Reynolds number of 1500, the trajectory of the blue dye was unable to bounce back in the second row. The vortical motion at the trailing edge of the vortex generator (Fig. 5(g)) is so strong that eventually mixes up with the blue dye. For a Reynolds number of 3300, the vortex strength is strong enough to make the flow relatively unsteady. In this Reynolds number, no distinct vortex pattern can be observed (see Figs. 5(h)–(j)). The blue dye behind the first row departing the first row is completely mixed up with the horseshoe vortex from the first row.

Fig. 6 shows the visual results of VG5 at $Re = 500$, 1500, and 3300. Note that the vortex angle for VG5 is 60° compared to VG1 of 30° . Basically, the phenomenon for VG5 is analogous to that of VG1 but accompanied with a much more intensified vortex strength. For instance, as seen from Figs. 6(a) and (b), one can see the trajectory of the red dye produces a relatively pronounced vortex motion. The circulation that appeared in plain fin geometry and in VG1 at $Re = 500$ is not seen. In addition, after hitting the vortex generator at the interception of first and second row, one can clearly see that the blue dye exhibits a vortex sheet and flows around the second row (Fig. 6(c)). More interestingly, part of the injected red dye at the left-hand side of the tube was sucked into the entrance of the second row (Fig. 6(c)). This phenomenon becomes even pronounced when the Reynolds number is further increased to 1500 (Fig. 6(f)). This implies the vortex strength for VG5 is

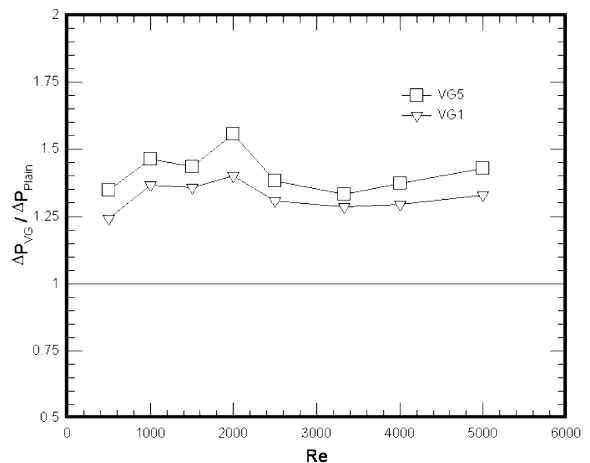
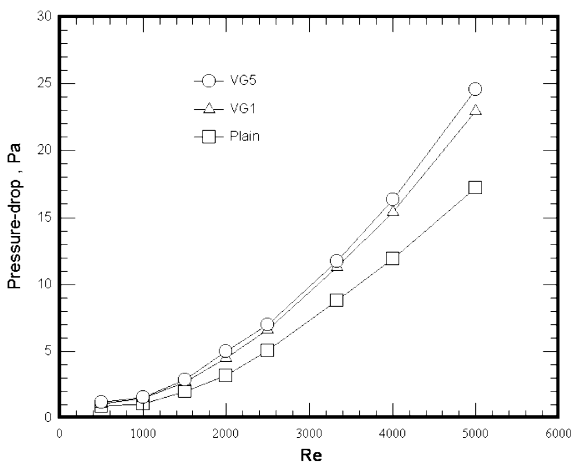


Fig. 8. Frictional performance for the plain, VG1, and VG5 vortex generators.

much larger than that of VG1, and providing better mixing characteristics of VG5. For VG5 at $Re = 1500$, the injected red dye produces strong motion that apparently induces the blue dye behind the tube and causing a very turbulent motion. In addition, as can be seen from Fig. 6(e), occasionally the injected red dye in the center position of inlet may be divided into two stream, one stream may be swirled into the stream at the edge of vortex generators and the other follows the horseshoe vortex that flows across the first row of the tube. For a Reynolds number of 3300, as shown in Fig. 6(g), even the injected dye from the wall position reveals strong vortical motions.

In summary, with the presence of vortex generator, the flow observation of the flow motions can be roughly described by Fig. 7. The horseshoe vortex that hits the first row will generate counter-rotating vortex, and the flow hits the first vortex generator also generates a pair of counter-rotating vortices. The pair of vortices will change their rotating direction when they flow across the second pair of vortex generator at the downstream. The corresponding pressure drops of the vortex generators and the plain fin geometry is shown in Fig. 8, from which the pressure drops for VG5 exceeds those of plain fin geometry by approximately 35–55%. The pressure drops for VG5 is about 10% higher than that of VG1. The penalty of pressure drops of the proposed vortex generators relative to plain fin geometry is relatively insensitive to change of Reynolds number. This is quite different from those interrupted surfaces that often shows consecutive increase of $\Delta P_{\text{int}}/\Delta P_{\text{plain}}$ vs. Reynolds number [11]. Although no heat transfer data were reported in this study, the flow patterns and the frictional performance of the vortex generators show promising prospective.

4. Conclusions

This study presents flow visualization and frictional results of enlarged fin-and-tube heat exchangers having inline arrangements. Tests are performed in a water tunnel by using dye-injection technique. Three samples of fin-and-tube heat exchanger are examined, including one plain fin and two wave-type vortex generators. Major conclusions of this study are summarized as follows:

1. For plain fin geometry at $Re = 500$, the horseshoe vortex generated by the tube row is not so pronounced, and a very large secondary flow circulation is seen in the interval of the first and the second row.
2. For plain fin geometry at $Re = 1500$, after hitting the first row of tube, the horseshoe vortex becomes more pronounced, and the flow circulation between the first and second row become larger and part of

the fluid is entrained to the horseshoe vortex. As the Reynolds number is increased to 3300, the strength of the horseshoe vortices is so large that the circulation region behind the tube starts to shed vortices.

3. With the presence of VG1 at a Reynolds number of 500, after hitting the first row, the horseshoe vortex becomes much more pronounced and the flow circulation behind the tube row is less profound. This flow circulation is completely eliminated for VG5 arrangement. In addition, the flow trajectory behind the first row for VG5 may even generate another pair of vortices when they flow across the vortex generators of the second row.
4. For VG5 arrangement, as the flow trajectory at the wall flows over the first row, it is found that the flow was sucked into the central region due to the strong strength of the vortices.
5. The frictional penalty of VG5 is about 10% higher than that of VG1 but the flow mixing characteristics for VG5 apparently outperforms that of VG1. The pressure drops for the wave type vortex generators are about 25–55% higher than those of the plain fin geometry. The penalty of pressure drops of the proposed vortex generators relative to plain fin geometry is relatively insensitive to change of Reynolds number.

Acknowledgements

The authors would like to express gratitude for the Energy R&D foundation funding from the Energy Commission of the Ministry of Economic Affairs, Taiwan.

References

- [1] ESDU 93024, Engineering Science Data Unit, 1993, Vortex Generators for Control of Shock-Induced Separation Part 1: Introduction and Aerodynamics.
- [2] M. Fibig, Vortices and heat transfer, *ZAMM Z. Angew. Math. Mech.* 77 (1) (1997) 3–18.
- [3] M. Fibig, Vortices, generators and heat transfer, *Trans. IChemE, A* 76 (1998) 108–123.
- [4] C.C. Wang, Technology review – a survey of the recent progress of the patents of fin-and-tube heat exchangers, *J. Enhanced Heat Transfer* 7 (2000) 333–345.
- [5] A.M. Jacobi, R.K. Shah, Heat transfer surfaces enhancement through the use of longitudinal vortices: a review of recent progress, *Exp. Thermal Fluid Sci.* 11 (1995) 295–309.
- [6] F.J. Edwards, G.J.R. Alker, The improvement of forced convection surface heat transfer using surfaces protrusions in the form of (A) cubes and (B) vortex generators, in: *Proceedings of the Fifth International Heat Transfer Conference*, Tokyo, vol. 2, 1974, pp. 244–248.

- [7] M. Fibig, P. Kallweit, N.K. Mitra, S. Tiggelbeck, Heat transfer enhancement and drag by longitudinal vortex generators in channel flow, *Exp. Thermal Fluid Sci.* 4 (1991) 103–114.
- [8] S. Tiggelbeck, N.K. Mitra, M. Fibig, Flow structure and heat transfer in a channel with multiple longitudinal vortex generators, *Exp. Thermal Fluid Sci.* 5 (1992) 425–436.
- [9] S. Tiggelbeck, N.K. Mitra, M. Fibig, Experimental investigations of heat transfer enhancement and flow losses in a channel with double rows of longitudinal vortex generators, *Int. J. Heat Mass Transfer* 36 (1993) 2327–2337.
- [10] S. Tiggelbeck, N.K. Mitra, M. Fibig, Comparison of wing-type vortex generators for heat transfer enhancement in channel flows, *J. Heat Transfer* 116 (1994) 880–885.
- [11] C.C. Wang, C.J. Lee, C.T. Chang, Some aspects of the fin-and-tube heat exchangers: with and without louvers, *J. Enhanced Heat Transfer* 6 (1999) 357–368.